Quantify the Abundance of Granite Composit Minerals Using the Hapke Model from Bidirectional Reflectance

Mengjuan Wu[1,2,3,4], Quan Wang[5,6], Jinlin Wang[1,2,3,4], Kefa Zhou[1,2,3,4], Zhixin Zhang[1,2,3,4], Xiumei Ma[1,2,3,4], and Weitao Chen[7]

[1]State Key Laboratory of Desert and Oasis Ecology, Xinjiang Institute of Ecology and Geography, Chinese Academy of Sciences, Urumqi, China

[2]Xinjiang Key Laboratory of Mineral Resources and Digital Geology, Chinese Academy of Sciences, Urumqi, China

[3]Xinjiang Research Centre for Mineral Resources, Chinese Academy of Sciences, Urumqi, China

[4]University of Chinese Academy of Sciences, Beijing, China

[5]Faculty of Agriculture, Shizuoka University, Shizuoka, Japan

[6]Research Institute of Green Science and Technology, Shizuoka University, Shizuoka, Japan

[7]School of Computer Science, China University of Geosciences, Wuhan, China

Corresponding authors: Quan Wang and Jinlin Wang (wang.quan@shizuoka.ac.jp, wangjinlin@ms.xjb.ac.cn)

Key Points:

- General spectral patterns and photometric parameters of natural granite, endmeber minerals, and their mixtures were retrieved from the bidirectional reflectance spectra measured at a range of incidence, emergence, and phase angles.
- Using the photometric parameters retrieved from multi-angle measurements as inputs to the Hapke model has accurately estimated the abundances and particle sizes of composits minerals for both natural and synthetic granite samples.
- Particle size and dark mineral (biotite) have little influence on the estimation accuracy.

Abstract

Quantitatively assessing the abundance of the composite minerals of terrestrial granite is crucial for understanding the evolutionary history of the Earth's crust and for mineral exploration. Prevalent methods based on the Hapke model to estimate mineral abundance by setting the optical constants of endmembers ahead are no longer applicable to terrestrial granite because of the complexity of natural granite, which will lead to remarkable uncertainties in estimations. In this study, we retrieved such specific photometric parameters from the bidirectional reflectance spectra measured at a range of incidence, emergence, and phase angles before they were inputted to the Hapke model to estimate mineral abundance. Four different kinds of granite samples of main rock-forming minerals (quartz, alkali feldspar, and plagioclase) comprising the bulk of granite were used to test the effectiveness of our proposed method. The effects of particle size and dark minerals on the inversion results using the visible near and shortwave infrared (VNIR-SWIR) wavelengths were also examined. The results show that using the photometric parameters retrieved from multiangle measurements as inputs for the Hapke model accurately estimated the abundances of quartz, alkali feldspar, and plagioclase for both natural and synthetic granite samples. Furthermore, the results also prove that the retrieved particle sizes of particulate samples are all within their measured ranges. These results indicate that the proposed approach provides a more accurate and efficient estimation of the compositions of terrestrial granite and is feasible for quickly assessing the abundance of minerals contained in granite.

1 Introduction

Granite consists essentially of quartz, alkali feldspar and/or plagioclase (Le Maitre, 1989) and is a major component of the Earth's crust (Bonin, 2012). Knowledge of granitic rocks contributes to understanding the evolutionary history of the Earth's crust, characterizing the crystal structure and compositional variation, and locating a series of ore deposits (such as gold, iron, copper, lead, and zinc) (Wang, 2015). To date, the traditional method used to identify and classify granite is based on a series of laboratory analyses, such as optical microscopy, X-ray fluorescence (XRF) analysis, and X-ray diffraction (XRD) analysis, which are time-consuming, often costly, and only applicable to limited samples collected from the field.

As a recent development, determining the abundance and distribution of rock composition over a large area through reflected information proves to be a quick and reliable method and is of increasing importance for geology and mineral exploration. Furthermore, absolute or relative estimations of the abundance of endmember minerals making up granite from the visible near and shortwave infrared (VNIR-SWIR) reflectance spectra may also provide important insights into the formation and evolution processes of granite. In general, qualitative methods used to characterize and classify different minerals use the diagnostic absorption features of the concerned minerals in the VNIR-SWIR region resulting from the molecular vibrational and electronic processes of water molecules, OH groups, and other bonds (Freek, 2018). Unfortunately, the spectra of granite lack unique diagnostic absorptions in the VNIR-SWIR region (Mustrad & Hays, 1997), and the endmember minerals (e.g. alkali feldspar and plagioclase) have often been considered spectrally transparent and almost featureless in this spectral domain (Serventi et al., 2013), leading the qualification to not be so straightforward. However, spectral 'unmixing' using radiative transfer models (RTMs) by considering all the influences of particle size and all endmembers, including spectrally neutral components, should

help to estimate the endmember minerals abundance of granite through the simultaneous fitting of reflectance values at many wavelengths (Robertson et al., 2016).

Two radiative transfer models commonly used in current remote sensing applications are those of Hapke (1993) and Shkuratov et al. (1999), both of which are mainly oriented for planetary bodies (Robertson et al., 2016). In comparison, the Hapke model (1993) considers multiangular measurements with the consideration of the incidence, emergence, and phase angles, while the Shkuratov et al. (1999) method is a simple one-dimensional geometrical-optics model based on the normal incidence and emittance angles used for calculating spectral albedo. Since reflectance spectra could vary with changes in illumination and viewing angles, the accurate estimation of mineral abundance using reflectance spectra would then rely heavily on light scattering models that quantitatively describe how light is scattered from the measured materials (Yang et al., 2019). In this context, the Hapke model is more appropriate for abundance estimation, and we only consider it in this study.

Previous studies suggest that the simplified Hapke model combined with a linear mixture model can estimate the abundance of minerals in intimate binary and ternary laboratory mixtures with reliable accuracies (Mustard & Pieters 1987a, 1989; Li & Milliken 2015; Robertson et al., 2016), and this approach has been widely applied to the Moon, Mars, and asteroids (Li & Milliken 2015; Poulet et al., 2002, 2010; Goudge et al., 2015； Liu et al., 2015; Lapotre et al., 2017); however, most geological materials analyzed to date are on mafic mineral mixtures (Mustard & Pieters, 1987a, 1987b, 1989; Li & Milliken, 2015) and less on rock-forming minerals. In this study, we specifically assessed the efficiency of the Hapke model for dealing with the nonlinearity of the spectral mixtures of main rock-forming minerals (quartz, alkali feldspar, and plagioclase) comprising the bulk of granite, as well as used only VNIR-SWIR wavelengths to study the effect of particle size and dark minerals on the inversion results. Note that the Hapke model (Hapke, 1993) has been fundamentally developed to explain the optical behavior of particulate mono-minerals or their mixtures, typically compact/loose powders (i.e., planetary regoliths) or atmospheres (De Angelis et al., 2017).

The procedure of spectral unmixing typically involves first decomposing into a collection of constituent spectra, or endmembers before determining the corresponding abundance of these endmembers (Keshava & Mustard, 2002). Thus, in this study, we built a spectral database of the main rock-forming minerals (endmember minerals) that are physically disaggregated from bulk granites based on laboratory bidirectional reflectance measurements. In previous studies, optical constants of endmembers retrieved from the Hapke/Shkuratov model were typically used as inputs to the Hapke model to estimate mineral abundance (Lucey, 1998; Li et al., 2015; Robertson et al., 2016; Warell & Davidsson, 2010), a step causing the largest source of uncertainty in the implementation of the Hapke model (Li et al., 2015). A study by Yang et al. (2019) on olivine, pyroxene, plagioclase, ilmenite, and their mixtures suggests that well-constrained photometric parameters retrieved from the Hapke model of the endmember minerals and their mixtures can help improve the accuracy of mineral abundance estimations.

Our analytical strategy used in this study is to examine the VNIR-SWIR reflectance spectra of the bulk slab and powder natural granite and the synthetic mixtures of endmember minerals (quartz, alkali feldspar and/or plagioclase). A previous study suggested that the differences with respect to particulate must be considered when this model is applied to bulk slab and powder surfaces of granite (De Angelis et al., 2017). Under a controlled laboratory setting, synthetic samples of a given mineral abundance and particle size for each component can be

prepared, enabling an assessment of the thresholds and accuracy evaluation. To improve the accuracy of mineral abundance estimations, the specific photometric parameters of a given sample used for the Hapke model are inversed alternatively based on the bidirectional reflectance spectra measured from a range of incidence, emergence, and phase angles in this study. These parameters are then inputted to the Hapke model as knowns to estimate the abundance of minerals. In detail, we assessed (1) the feasibility and accuracy of the proposed approach to derive the known mineral abundance for both natural granite and synthetic mixtures of endmember minerals using VNIR-SWIR reflectance spectra; and (2) the influence of particle size and dark minerals on the estimation accuracy.

2 Materials and Methods

2.1 Sample Preparation and Spectral Measurements

The samples used in this paper are from the same area as those used in Wu et al. (2020), in which the general background of the research area was introduced. Furthermore, a detailed description of measuring the spectral data of natural granite samples has also been provided in Wu et al. (2020).

2.1.1 Endmember Minerals

Estimating the abundance from the Hapke model requires an endmember spectral library of each mixture. As revealed above, the primary minerals relevant to natural bulk granite are Qtz, Pl, and Kfs. The endmember mineral of biotite was also extracted to reveal the influence of dark minerals on the inversion. We prepared mineral samples from three large bulk granite pieces, which were used to separate the crystals of the endmember minerals and sieved to different sizes (Fig. 1). The rock sorting process was carried out in a professional appraisal agency (Integrity Geology Services Limited) for grinding and sieving.

Different endmember minerals were prepared using different methods. For instance, electromagnetic minerals, e.g., biotite, were separated by electromagnetic selection, feldspar and quartz were sieved by flotation, feldspar was separated into plagioclase, and K-feldspar was finally separated by a dense liquid method. The purity of each endmember mineral was again determined by XRD analyses (Table 1). There were only minor composition differences for different Qtz and Pl endmembers, but the compositions of different Kfs endmembers were markedly different. The compositions of Kfs1-Kfs3 include mainly Kfs and Mc, while those of Kfs4-Kfs8 are mainly Pl and Mc.

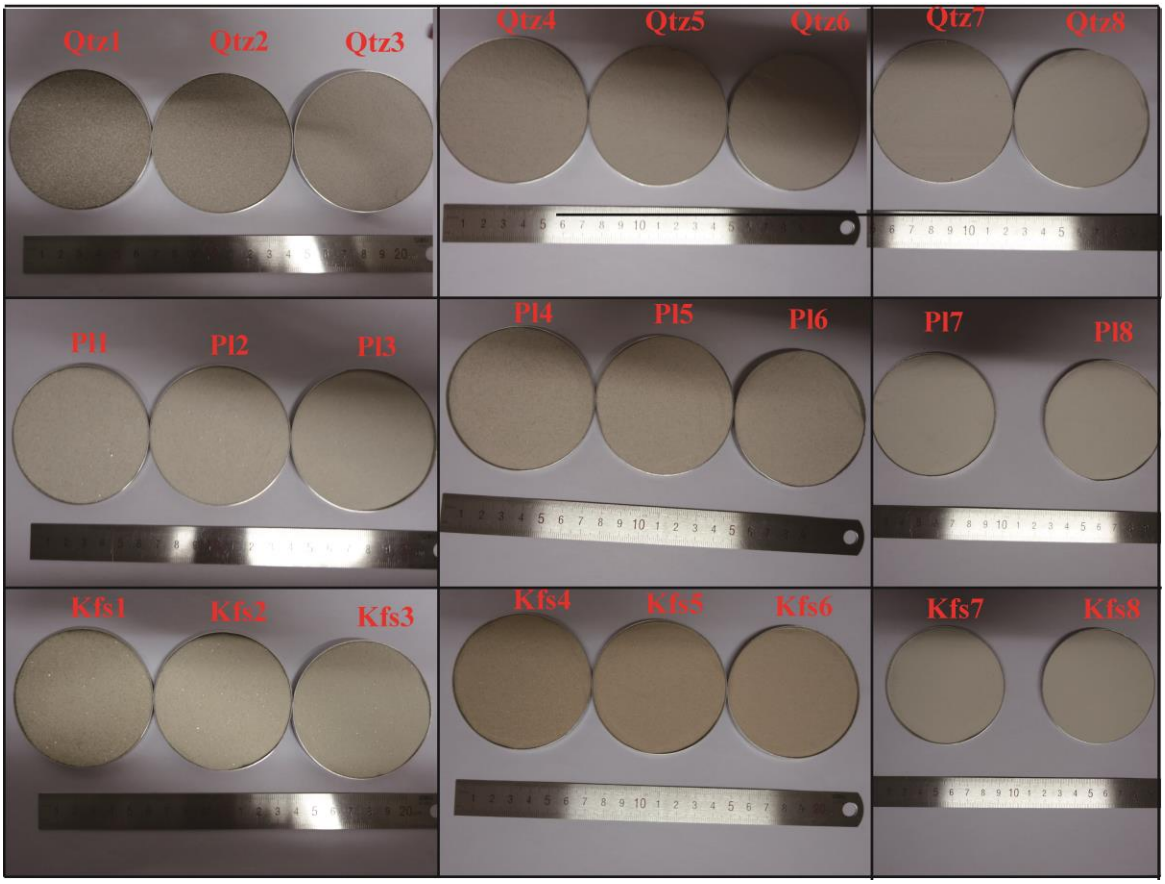

Figure 1. Endmember minerals separated from three granite pieces (each column corresponds to one sample). Qtz-quartz; Pl-plagioclase; Kfs-K feldspar. The particle size of the endmembers are as follows: Qtz1, Pl1, Kfs1: 250-380 μm; Qtz2, Pl2, Kfs2: 180-250 μm; Qtz3, Pl3, Kfs3: 150-180 μm; Qtz4, Pl4, Kfs4: 120-150 μm; Qtz5, Pl5, Kfs5: 109-120 μm; Qtz6, Pl6, Kfs6: 96-109 μm; Qtz7, Pl7, Kfs7: 80-96 μm; Qtz8, Pl8, Kfs8: 75-80 μm.

Table 1. *Mineral Abundance in All Endmember Minerals Determined from XRD Analyses.*

Sample ID	Mineral Abundance (%)					
	Qtz[1]	Pl[2]	Kfs[3]	Mc[4]	Chl[5]	Bt[6]
Qtz1-Qtz3	99	1	0	0	0	0
Qtz4-Qtz6	100	0	0	0	0	0
Qtz7-Qtz8	98	1	1	0	0	0
Pl1- Pl3	6	94	0	0	0	0
Pl4- Pl6	5	95	0	0	0	0
Pl7- Pl8	6	94	0	0	0	0
Kfs1- Kfs3	8	19	73	0	0	0
Kfs4- Kfs6	6	22	0	72	0	0
Kfs7- Kfs8	0	13	0	87	0	0
Bt	0	0	0	0	4	96

Note. [1] Qtz-quartz; [2] Pl-plagioclase; [3] Kfs-K-feldspar; [4] Mc-microcline; [5] Chl-chlorite; [6] Bt-biotite.

2.1.2 Mixtures of Endmember minerals

To verify the effectiveness of the Hapke model to retrieve the abundance of rock-forming minerals of granite, the endmember minerals were mixed by stirring and shaking to produce ternary mixtures with 0, 15, 30, 45, 60, 75, and 100 wt. % plagioclase in proportion to feldspar according to the QAPF (Q-quartz, A-alkali-feldspar, P-plagioclase, F-feldspathoids) double-triangle diagram (Streckeisen, 1968) recommended by the International Union of Geological Sciences (IUGS). Furthermore, to study the effect of particle size on the inversion results, we prepared mixtures of three different particle size ranges (250-380 μm, 120-150 μm, and 75-80 μm) for each of the different contents of dark minerals (e.g., biotite) that were additionally added into the ternary mineral mixtures to examine their its influence on the abundance inversion. The detailed configuration is shown in Table 2.

Spectra of these mixtures provide perfect scenarios for testing the RTMs because important variables (mineral abundance and mean particle sizes) are known (Li et al., 2015). The results obtained from these idealized cases can then be compared to results from natural bulk granite to understand the likely sources of uncertainty when applying the models to more complex natural systems.

Table 2. *Actual Mass Fractions of Each Mixture Composed of Endmember Minerals.*

Mixture ID	Endmember Minerals			Mass Fraction (%)			Biotite Mass Fraction[1] (%)
EM101	Qtz1	Pl1	Kfs1	25.00	0.00	75.00	0.00
EM102	Qtz1	Pl1	Kfs1	25.00	11.25	63.75	0.00
EM103	Qtz1	Pl1	Kfs1	25.00	22.50	52.50	0.00
EM104	Qtz1	Pl1	Kfs1	25.00	33.75	41.25	0.00
EM105	Qtz1	Pl1	Kfs1	25.00	45.00	30.00	0.00
EM106	Qtz1	Pl1	Kfs1	25.00	56.25	18.75	0.00
EM107	Qtz1	Pl1	Kfs1	25.00	75.00	0.00	0.00
EM108	Qtz1	Pl1	Kfs1	25.00	33.75	41.25	1.00
EM109	Qtz1	Pl1	Kfs1	25.00	33.75	41.25	2.00
EM110	Qtz1	Pl1	Kfs1	25.00	33.75	41.25	3.00
EM111	Qtz1	Pl1	Kfs1	25.00	33.75	41.25	4.00
EM112	Qtz1	Pl1	Kfs1	25.00	33.75	41.25	5.00
EM201	Qtz4	Pl4	Kfs4	35.00	0.00	65.00	0.00
EM202	Qtz4	Pl4	Kfs4	35.00	9.75	55.25	0.00
EM203	Qtz4	Pl4	Kfs4	35.00	19.5	45.50	0.00
EM204	Qtz4	Pl4	Kfs4	35.00	29.25	35.75	0.00
EM205	Qtz4	Pl4	Kfs4	35.00	39.00	26.00	0.00
EM206	Qtz4	Pl4	Kfs4	35.00	48.75	16.25	0.00
EM207	Qtz4	Pl4	Kfs4	35.00	65.00	0.00	0.00
EM208	Qtz4	Pl4	Kfs4	35.00	29.25	35.75	1.00
EM209	Qtz4	Pl4	Kfs4	35.00	29.25	35.75	2.00
EM210	Qtz4	Pl4	Kfs4	35.00	29.25	35.75	3.00
EM211	Qtz4	Pl4	Kfs4	35.00	29.25	35.75	4.00
EM212	Qtz4	Pl4	Kfs4	35.00	29.25	35.75	5.00
EM301	Qtz8	Pl8	Kfs8	45.00	0.00	55.00	0.00
EM302	Qtz8	Pl8	Kfs8	45.00	8.25	46.75	0.00

EM303	Qtz8	Pl8	Kfs8	45.00	16.50	38.50	0.00
EM304	Qtz8	Pl8	Kfs8	45.00	24.75	30.25	0.00
EM305	Qtz8	Pl8	Kfs8	45.00	33.00	22.00	0.00
EM306	Qtz8	Pl8	Kfs8	45.00	41.25	13.75	0.00
EM307	Qtz8	Pl8	Kfs8	45.00	55.00	0.00	0.00
EM308	Qtz8	Pl8	Kfs8	45.00	24.75	30.25	1.00
EM309	Qtz8	Pl8	Kfs8	45.00	24.75	30.25	2.00
EM310	Qtz8	Pl8	Kfs8	45.00	24.75	30.25	3.00
EM311	Qtz8	Pl8	Kfs8	45.00	24.75	30.25	4.00
EM312	Qtz8	Pl8	Kfs8	45.00	24.75	30.25	5.00

Note. [1] Biotite separated from the first sample, and the grain size is 150-380 μm.

2.1.3 Measurement of the Bidirectional Reflectance Spectra

The bidirectional reflectance spectra of all samples were measured using the Northeast Normal University Laboratory Goniospectrometer System (NENULGS), consisting of a goniometer, artificial illumination, and an ASD FieldSpec3 spectroradiometer. Details of this system can also be found in Sun et al. (2014). The placement of the slab and powder samples and the detailed observation angle setting can be found in Wu et al. (2020).

2.2 Spectral Unmixing Using the Hapke Model

Unmixing methods based on radiative transfer theory exploit the fact that although reflectance is not linearly correlated with a concentration in a mixed spectrum, the bulk single scattering albedo (SSA) or the probability that a photon will survive the interaction with a particle is a linear combination of the SSAs of the minerals in the mixture (Sklute, 2015). Using the Hapke model (1993), we assumed that the mean SSA of a mixture is a linear combination of the single-scattering albedos of the endmember components weighted by the relative geometric cross section of that component according to Mustard and Pieters (1987). The equation describing this can be represented as

$$\omega_{ave}(\lambda) = \frac{\sum \omega_i(\lambda)(M_i/\rho_i d_i)}{\sum(M_n/\rho_n d_n)}, \quad (1)$$

where ω_i, M_i, ρ_i, and d_i are the SSA, bulk density, solid density, and particle effective diameter of endmember *i*, respectively. The coefficient by which the single scattering albedo spectrum of endmember *i* in the mixture is weighted as

$$F_i = \frac{M_i/\rho_i d_i}{\sum(M_n/\rho_n d_n)}, \quad (2)$$

where F_i is the relative geometric cross-section of endmember *i* (Mustard & Pieters, 1987). In this study, the particle sizes of all the endmembers and mixtures are the same, and the solid densities of all the endmembers are similar. Consequently, the F-parameter can be taken as the mass fraction (Hapke, 1993).

The Hapke model has evolved over the years from the isotropic multiple-scattering approximation model (IMSA) to the anisotropic multiple-scattering approximation model (AMSA) and, eventually, to H2008 (including porosity effects) (Hapke, 2008). Following Yang et al. (2019), we employed the same model in this study, in which the reflectance is described as

$$r(i,e,g) = \frac{\omega_{ave}}{4\pi}\frac{\mu_0}{\mu_0+\mu}\left[\left(1+B(g)\right)p(g) + H(\mu,w)H(\mu_0,w) - 1\right], \quad (3)$$

where μ_0 and μ are the cosine of the incidence and emergence angle, respectively. $B(g)$ is the back scattering function, $p(g)$ is the phase function, and $H(x,w)$ is the multiple scattering function which is described by Ambartsumian-Chandrasekhar's H-function (Chandrasekhar, 1960).

The $p(g)$ is modeled by a double Henyey-Greenstein (HG) function (Hapke, 1993):

$$P_{HG}(g) = \frac{1+b}{2}\frac{1-c^2}{[1+2c\cos g+c^2]^{3/2}} + \frac{1-b}{2}\frac{1-c^2}{[1-2c\cos g+c^2]^{3/2}}, \quad (4)$$

where *b* describes the angular width of the scattering lobe, and *c* describes the amplitude of the backscattered lobe relative to the forward lobe. We first simultaneously estimate the values of the single scattering albedo (ω) and parameters (*b* and *c*) in $P_{HG}(g)$ for all samples by fitting the spectra measured at different angles using equations (3) and (4). Since the BRFs used in the spectra fitting were measured at phase angles $g \geq 30°$, we assumed $B(g) = 0$. Meanwhile, we adopted the same method used in Yang et al. (2019) to find the best fit values of ω, *b*, and *c*, which are endmember specific and wavelength dependent. Thus, the values of ω, *b*, and *c* were used as known inputs into the Hapke model, which can be solved inversely to estimate the abundance and particle size of each endmember component at the standard viewing geometry of i=30°, e=0° using the constrained particle swarm optimization (CPSO) method (Chen, 2020) and the least square criterion by minimizing the difference between fitted and measured reflectance spectra. In the solutions, the sum of the mass fractions determined by the model is forced to sum to unity within the constrained method. Finally, the mineral abundance derived from the bidirectional reflectance spectra of natural bulk granite and mixtures of endmember minerals were compared and used to examine the validity and accuracy of the approach.

3 Results

3.1 General Spectral Patterns of Natural Granite, Endmember Minerals, and Their Mixtures

The reflectance spectra of each endmember mineral and their mixtures are presented in Fig. 2, while the spectra of the bulk slab and powder natural granite samples have been reported in Wu et al. (2020). The spectral profiles of the bulk powder granite are similar, with prominent spectral absorption features located at 0.40 μm, 1.40 μm, 1.90 μm, and 2.22 μm. However, the spectral patterns of bulk slab granite are different for each hand specimen. In addition, the spectra of natural granite also have gentle absorption features at 2.23 μm and near the wavelength domain from 2.3 to 2.5 μm (Wu et al., 2020).

Spectra of the same endmember mineral type exhibit strong similarities, even though they are separated individually from different granite pieces, except for the plagioclase endmember separated from the first granite piece (Pl1-Pl3) (Fig. 2a), whose spectra present a absorption band at 1.25 μm that is unique compared to other Pls endmembers' spectra. The reflectance spectra of Qtzs, Pls, and Kfss show similar absorptions at 0.4 μm, 1.4 μm, and 1.9 μm. However, the absorption band at 2.2 μm was also observed in the Pls endmembers. In comparison, the reflectance spectra of biotite are flat and low, lacking distinctive absorption features.

The bidirectional reflectance spectra of all the endmember mixtures exhibit the expected patterns concerning both the absorption band depth and position for each particle size (Fig. 2b-d). Most notably, there were large decreases in the reflectance values obtained for the ternary mixtures with increasing contents of biotite regardless of the particle size of the mixtures. The spectral profiles of the endmember mixtures containing biotite are more similar to those of natural granite, indirectly suggesting that the natural granite contains dark minerals, e.g., biotite. The absolute reflectance values obtained for natural granite, endmember minerals, and their mixtures at different particle sizes show that as particle size coarsens, the reflectance values decreased systematically (Fig. 2).

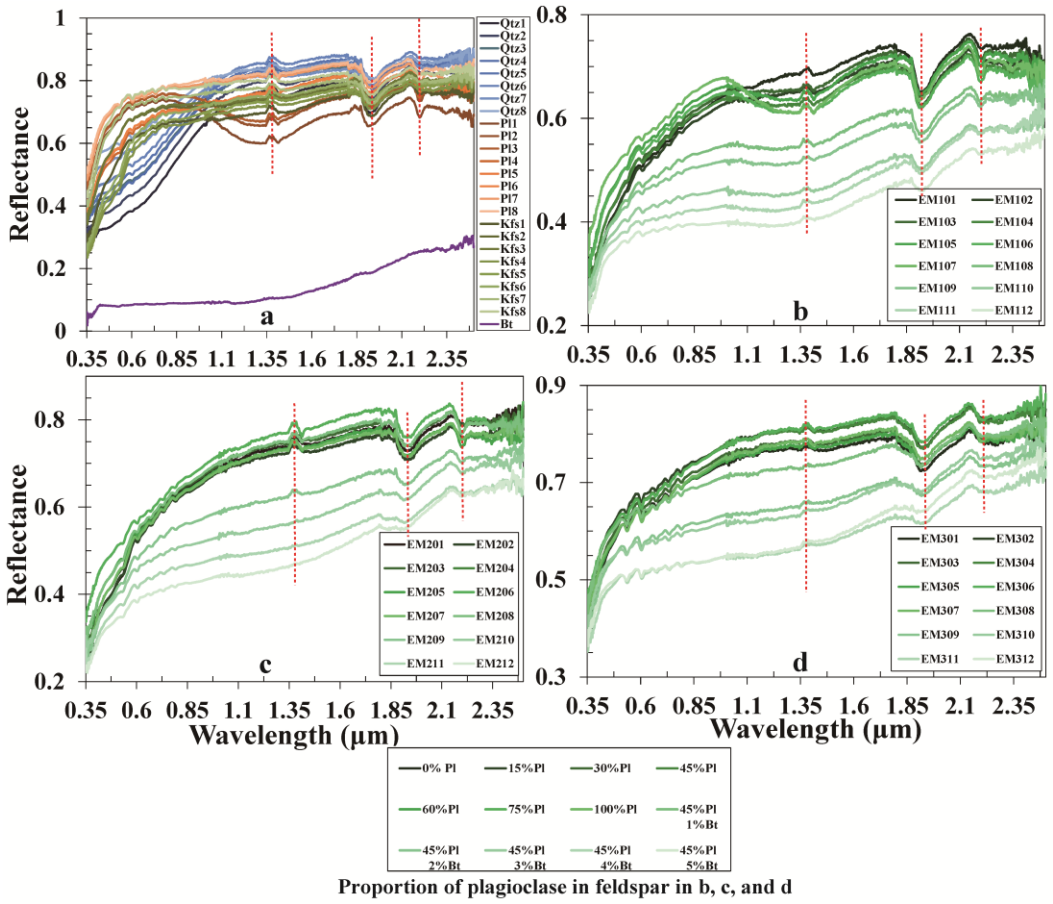

Figure 2. Bidirectional reflectance spectra of endmember minerals and their mixtures with different particle sizes, measured with an incidence angle of 30° and an emergence angle of 0°. a. Separate endmember minerals; b. endmember mixtures of Qtz1, Pl1, Kfs1, and Bt; c. endmember mixtures of Qtz4, Pl4, Kfs4, and Bt end-members; d. endmember mixtures of Qtz8, Pl8, Kfs8, and Bt.

3.2 Derivation of the Photometric Parameters

To obtain the photometric parameters required by the Hapke model for estimating mineral abundance, we first calibrate the simplified Hapke model and the $P_{HG}(g)$ through multiangle measurements. For simplification, we only selected the samples of endmember minerals and their mixtures to present the derived SSA values, and the *b*, and *c* coefficients of

the $P_{HG}(\mathrm{g})$ function in Fig. 3-4. Since the derived photometric parameters (ω, b, and c) of the natural granite samples were given in Wu et al. (2020), the Pls series and EM1 series have been selected to present parameter ω for illustration (Fig. 3). The SSA spectra of all samples evolve with wavelength, which is consistent with the reflectance spectrum, with in which the minima and maxima of ω correspond to the minima and maxima of the spectrum. As expected, the characteristic of the reflectance is also shown in the SSA spectra in that the values of ω increase when the particle sizes decrease.

The scattering properties of the measured sample can be characterized by the coefficients b and c of the $P_{HG}(\mathrm{g})$ function. The values of parameter b range from 0.05 to 0.2 for natural granite samples set over the 0.35-2.5 μm spectral range, and the parameter c values remain almost constant at -1 (Wu et al., 2020). The endmember minerals and their mixtures yield b and c values that are similar to those of natural granite samples. The b and c values obtained for all samples are not wavelength dependent. Thus, to display the data more concisely, we calculate the average values of b and c at each wavelength for each sample set, e.g., endmember minerals and their mixtures, as shown in Fig. 4, over the entire wavelength range. The negative c values imply that there is a strong forward scattering characteristic, which has been found for all measured samples.

The quality of the fits of the measured and modeled bidirectional reflectance at the standard angle (θ_i=30°, θ_e=0°, and g=30°) for all samples is determined from the root mean square error (*RMSE*) between the actual and calculated curves. The calculated *RMSEs* are below 1×10^{-4} for endmember minerals and their mixtures, and the *RMSEs* of natural granite samples fall inside a range from 0.006 to 0.05, which is similar to the expected experimental errors. For endmember minerals, the fits generally agree well at all wavelengths. In comparison, the spectral fits obtained for natural granite and endmember mixtures are also good but with higher residuals in the 0.35 μm - 0.9 μm region.

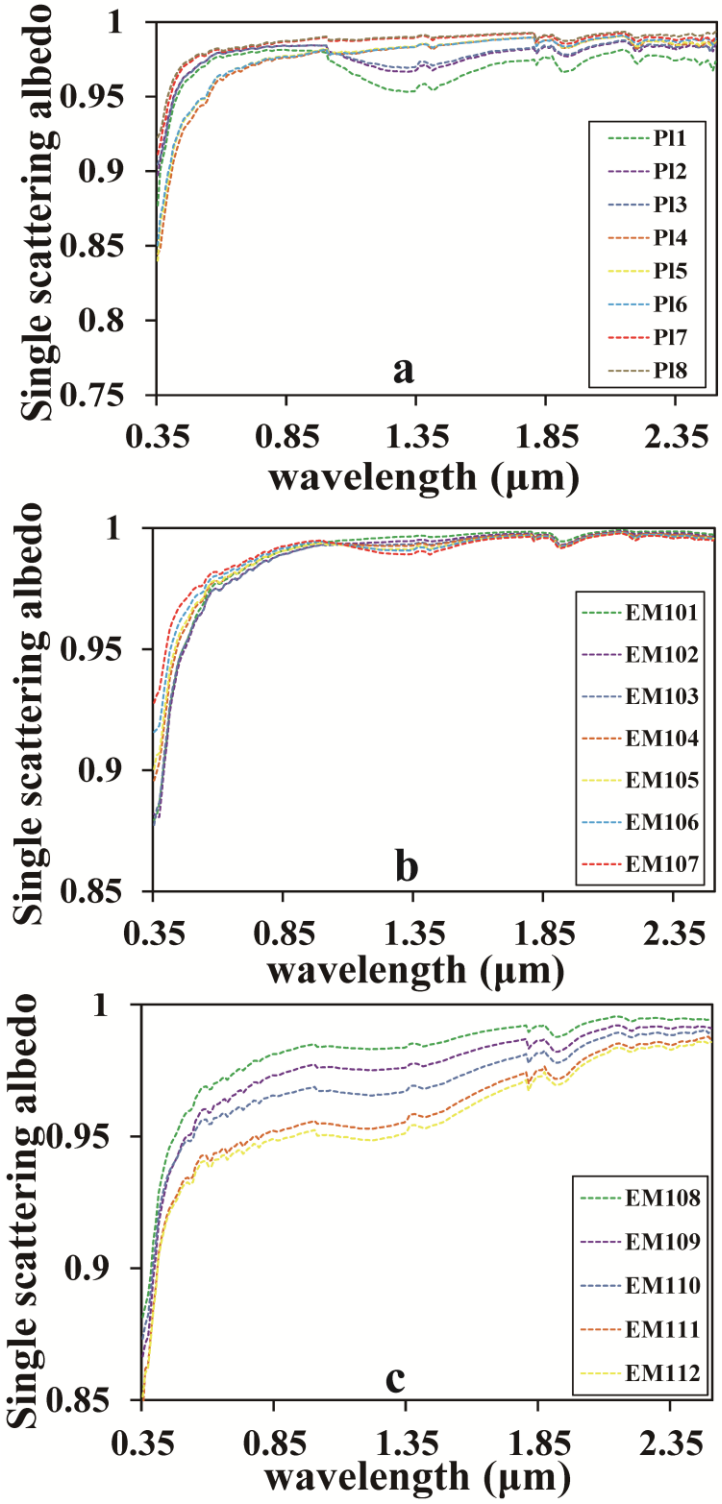

Figure 3. Photometric parameter of ω retrieved for the Pls series (a) and EM1 series (b, c) over the VNIR-SWIR spectral range.

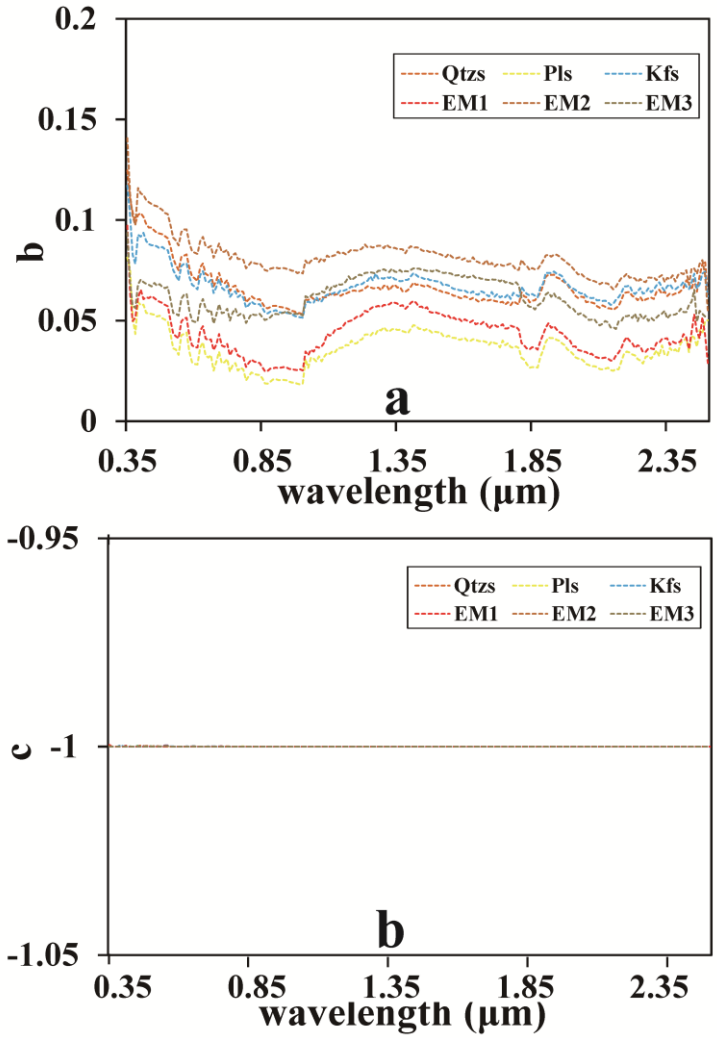

Figure 4. The average values of retrieved photometric parameters b and c at each wavelength for each sample set, e.g., endmember minerals and their mixtures over the VNIR-SWIR spectral range.

3.3 Spectral Unmixing

As stated above, the outputs of equations (1) and (3) include the estimation of particle size and weighting coefficient (F-parameter) solved using the CPSO method for the measured and computed bidirectional reflectance spectra at the standard angle. We present here two different scenarios from natural granite and endmember mixtures. The estimated results of mineral abundance are shown in Fig. 5 and Fig 6. Fig. 6 shows a graphical representation of the actual and calculated mass fraction obtained for ternary mixtures of quartz, plagioclase, and K-feldspar, allowing a rapid qualitative assessment of the accuracy of the fit as well as any systematic deviation present in the results. The estimated particle sizes and *RMSE* obtained for each sample are presented in Table 3.

For the endmember mixtures with known endmember reflectance spectra and particle diameters (EM1, EM2, and EM3), the accuracy of the mineral abundance estimation in most intimate mixtures is within 10% (absolute), as revealed in Fig. 6. Meanwhile, the accuracy of the

computed abundance increases with decreasing particle size. The abundance estimates obtained for the 75-80 μm size fraction (EM3) are nearly all within 5% of the measured values, while for most samples in the 120-150 μm size fractions (EM2), they are within the range of 5-10%. The abundances calculated for biotite-bearing mixtures are as accurate as those calculated for the nonbiotite-bearing endmember mixtures, except for the EM1 series (250-380 μm), which has an accuracy < 10% for biotite-bearing mixtures. The spectral fit between the measured and calculated reflectance of the biotite-bearing mixtures is worse than the fit obtained for the mixtures without biotite, which is clearly reflected in the *RMSE* values (Table 3). For the EM1 series, the greatest mismatches between the measured and modeled mixture spectra occur near wavelengths of 1.4 μm and 1.9 μm.

On the other hand, for the bulk slabs and unsorted powders of natural granite samples, the abundance inversion is not as accurate as that obtained for the endmember mixtures of the EM2 and EM3 series. The abundance estimated for bulk powders of natural granite generally have errors within 10%, while the agreement between the calculated and actual abundances of the bulk slab natural granites could be larger than 10%, with a maximum error reaching 19%. The mismatches of the reflectance spectra are more prominent for natural granite samples, as indicated by the *RMSE* values (varying from 0.11 to 0.16).

The estimation error of quartz is better than 5% for most endmember mixtures without biotite, while plagioclase and K-feldspar have slightly worse estimations of mineral abundance. The mismatches of plagioclase and K-feldspar are systematic, with most of the results underestimating the content of K-feldspar while overestimating the content of plagioclase. This trend did not appear in biotite-bearing mixtures, e.g., endmember mixtures with biotite and natural granite.

The particle sizes of each sample retrieved from the Hapke model are also presented in Table 3. The retrieval was based on the assumption that the particle size of each endmember mineral in the mixtures is the same, and the modeled particle size is the average value of the measured sample. The actual particle size is based on the reported sieve mesh size used during sample preparation (Table 3). The particle size estimated for most particulate samples is within the actual particle size range (Table 3). The estimated grain size falls on the upper boundary of the actual particle range. In the endmember mixtures, the retrieved particle size of different samples in the same series has a very slight difference (Table 3).

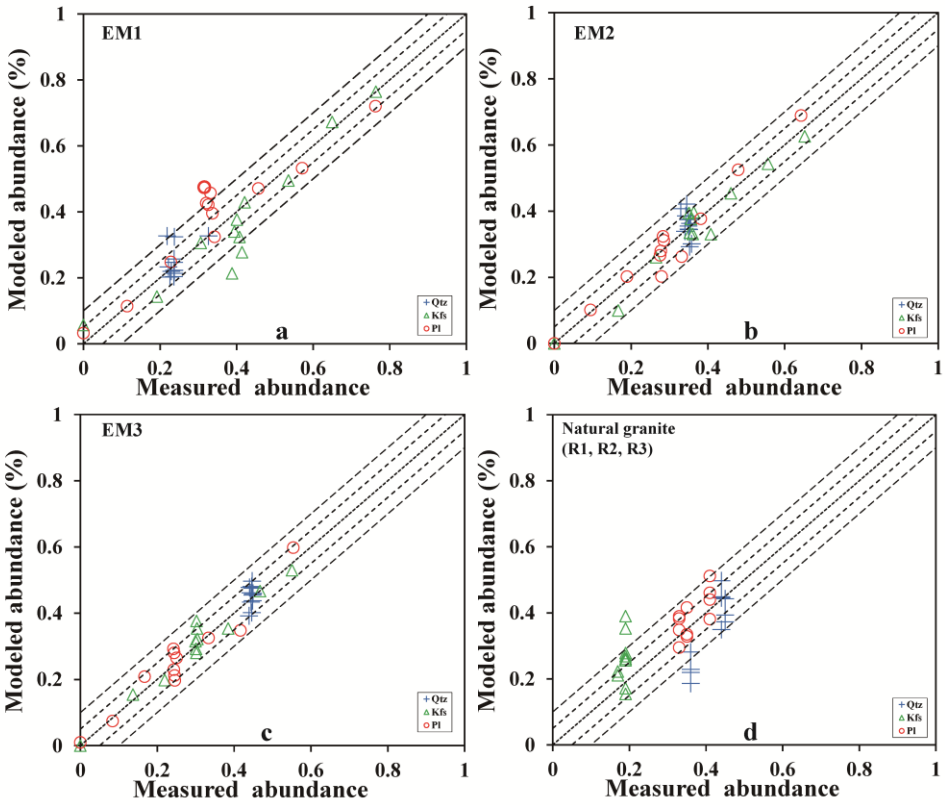

Figure 5. F-parameter plots obtained for a. EM1, b. EM2, and c. EM3 endmember mixture series and d. R1, R2, and R3 natural granite.

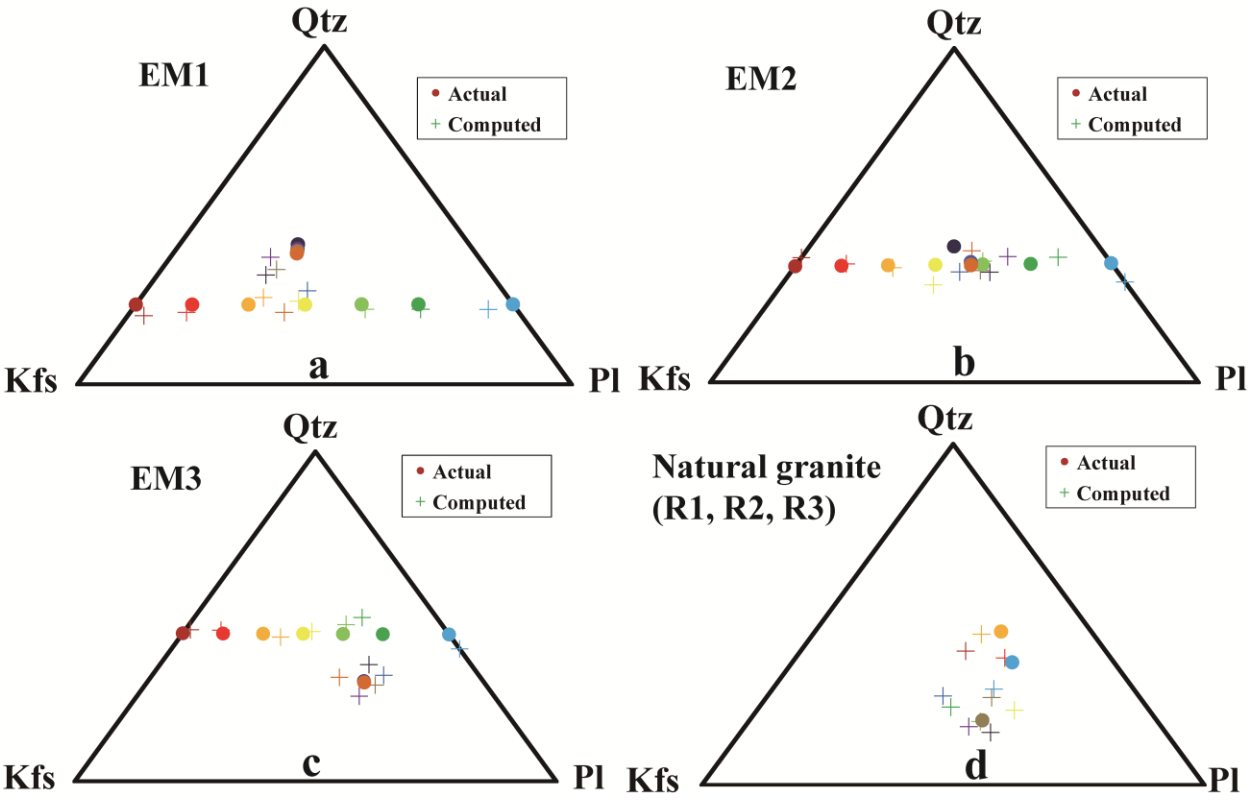

Figure 6. Results of mineral mixture modeling for the endmember mixtures and natural granite for the three-component mixtures. The proportion of each endmember required to minimize the error of the fit is used to determine the F-parameters as a cross. The actual F-parameters are shown by the solid circles on the same plot. The vertices of this ternary diagram represent 100% of the components quartz (Qtz), plagioclase (Pl), and K-feldspar (Kfs).

Table 3. *Actual and Computed Particle Size (μm).*

Mixture ID[1]	Actual	Computed[2]	SD[3]
EM101	250-380	374.05	0.14
EM102	250-380	379.34	0.10
EM103	250-380	369.56	0.10
EM104	250-380	379.47	0.10
EM105	250-380	377.31	0.07
EM106	250-380	358.89	0.09
EM107	250-380	315.40	0.09
EM108	250-380	345.32	0.10
EM109	250-380	375.62	0.10
EM110	250-380	378.48	0.13
EM111	250-380	373.45	0.13
EM112	250-380	379.74	0.14
EM201	120-150	198.16	0.07
EM202	120-150	192.30	0.09
EM203	120-150	192.75	0.11
EM204	120-150	195.98	0.11
EM205	120-150	196.19	0.10
EM206	120-150	194.07	0.11
EM207	120-150	199.68	0.11

EM208	120-150	196.08	0.12
EM209	120-150	196.98	0.13
EM210	120-150	194.39	0.13
EM211	120-150	191.06	0.14
EM212	120-150	189.93	0.15
EM301	75-80	117.41	0.06
EM302	75-80	116.46	0.06
EM303	75-80	119.35	0.06
EM304	75-80	117.27	0.06
EM305	75-80	116.47	0.06
EM306	75-80	117.24	0.07
EM307	75-80	117.48	0.07
EM308	75-80	118.42	0.11
EM309	75-80	119.62	0.11
EM310	75-80	112.94	0.11
EM311	75-80	118.97	0.11
EM312	75-80	119.71	0.14
R101	slab	+∞	0.11
R102	250-380	334.05	0.16
R103	180-250	242.14	0.16
R201	slab	+∞	0.11
R202	150-180	192.86	0.14
R203	120-150	196.67	0.13
R204	109-120	143.22	0.14
R301	slab	+∞	0.11
R302	96-109	146.06	0.13
R303	80-96	146.68	0.13
R304	75-8	146.32	0.11

Note. [1] The selection of endmember spectra in the samples uses the mineral endmember with the corresponding particle size in the endmember library; [2] the particle size is the average particle diameter; [3] the *RMSE* was calculated using the wavelength region 0.35 to 2.50 μm.

4 Discussion

4.1 Spectral and Photometric Properties of Synthetic (endmember mixtures) and Natural Granite Samples

The spectral patterns closely matched, so the inferred mineralogies of the synthetic (endmember minerals) and natural granite samples are obtained in this study. Theoretically, the absorption features below 0.6 μm (and even into the ultraviolet domain) may result from several different kinds of electronic charge transitions and charge transfers involving iron or other transitions. However, the existence of K-feldspars that have Fe3+ absorptions below 0.5 μm (Adams, 1974) or thin mineral coatings of iron oxides in natural granite accounts for the pattern obtained in this study. The separated K-feldspar endmember has a pink color, which is caused by the strong absorption of blue light by Fe3+. Biotite also has absorptions at 0.5 μm and 0.71 μm, which are probably Fe^{2+} and Fe^{2+} - $Fe3^{+}$ charge transfer features (Adams, 1974). On the other hand, the presence of water bands (1.4 and 1.9 μm) is due to trapped and/or adsorbed water of quartz, plagioclase, and K-feldspars (Adams, 1974). The 1.4 μm band is produced by a combination of symmetric OH stretching and asymmetric OH stretching, while the 1.9 μm band is attributed to HOH bending in addition to asymmetric OH stretching (Hunt, 1977). As shown in Wu et al. (2020), natural granite has a unique absorption at 2.3 μm compared with the synthetic samples (Fig. 2a) due primarily to the existence of alteration minerals in natural granite, which is

a combination band involving the OH fundamental stretching mode and the fundamental AlOH bending mode (Adams & Goullaud, 1978). According to the petrographic analysis of thin sections of all samples, most of the plagioclase in natural granite showed sericitization and kaolinization.

Furthermore, the reflectance values of endmember mixtures and natural granite increase simultaneously with decreasing of particle size, consistent with a previous report (Adams & Filice, 1967). Although the content of biotite in the synthetic granite is low, with a mass fraction ranging from 1% to 5%, the overall reflectance values of synthetic granite samples have been greatly reduced, suggesting that they are strongly controlled by biotite. This phenomenon echoes a well-known discovery that the reflectance level was controlled by the darkest grains in intimate mixtures (Gaffey, 1986; Cloutis et al., 1990a, 1990b; Britt & Pieters, 1989; Britt, 1991; Clark, 1983). Thus, the spectral profile of biotite-bearing endmember mixtures is closer to that of natural granite due to the existence of biotite in natural granite.

For all samples, the calculated single scattering albedo (ω) is sensitive to the variation in grain size, while the derived parameters *b* and *c* in the phase function have shown good agreement regardless of whether the measured sample contains biotite. As indicated by the values of parameter *b*, the measured reflectance values are greater in forward scattering mode. This is because in the case of intimate mixtures, the phase curve forward/backward scattering properties are driven by the most abundant, brightest, and highly anisotropic scattering grains (Pilorget et al., 2015). Consequently, the scattering characteristics of endmember mixtures and natural granite are consistent with those of Qtz, Kfs, and Pl, which account for more than 95% of the samples in this study.

The different spectral characteristics and photometry properties of the synthetic (endmember minerals) samples and natural granite imply that the synthetic granite composed of simple endmember minerals is unlikely to represent the bulk effect of a natural granite surface. Thus, our study clearly indicates the limitations of only using particulate minerals (synthetic granite) measured in the laboratory to model natural mineral assemblages.

4.2 Spectral Fits

The spectral fitting results show that a significant difference may occur when using the multi- or monoangular results retrieved from the Hapke model. As shown in Fig. 5, spectral fitting at the standard angle (θ_i=30°, θ_e=0°, and g=30°) of all samples exhibits a high fitting accuracy when using the multiangular bidirectional reflectance. However, when using the reflectance measured at the standard angle only to estimate the mineral abundances and particle sizes, the differences between modeled and measured spectra increase significantly, especially when the samples contain biotite (Table 3). This clearly indicated that the multiangular measurements could have provided a detailed and reliable description of terrestrial surfaces and are more capable of resolving the physical and chemical characteristics of measured samples than single-angle measurements, which are usually nadir measurements (Hapke, 1993; Jacquemoud et al., 1992). In addition, the good spectral fitting results retrieved from the multiangular measurements have shown that the angular domain of our observation settings was sufficiently large to confidently determine the values of Hapke's photometric parameters, which can be effectively used to retrieve the photometric properties of sample surfaces.

When using the monoangular measurements to estimate the mineral abundance, we forced the F-parameters of any mixture to be summed to 1. According to Mustard and Pieters (1987), the abundances calculated when the F-parameters are forced to sum to unity are in significantly better agreement (to within 3%), but the error of the spectral fitting is 2 to 4 times worse than that when using the unconstrained fits. In this study, we sacrificed the quality of the spectral fit to obtain a highly accurate abundance estimation, leading to poor spectral fitting using the monoangular retrieved parameters. However, if such a restriction is removed, the accuracy of the unconstrained fits can improve significantly, with the spectral fit accuracy of the endmember mixtures still being acceptable without biotite. On the other hand, the presence of biotite in endmember mixtures and natural granite, a phase that can act as an effective and nonlinear darkening agent (Li & Milliken, 2015), greatly reduces the fitting accuracy. We have not included biotite in our input library of mineral endmembers in this study, and the spectral fits of endmember mixtures may significantly be improved by the inclusion of biotite as an endmember, which deserves to be evaluated in future studies. Furthermore, when the Hapke model is applied to the slab or unsorted grains of natural granite, imperfect knowledge of the scattering properties of the endmembers may also produce unreasonable values or large errors for spectral fitting.

4.3. Estimates of mineral abundance

The F-parameters of endmember minerals in measured samples were forced to be summed to 1 to obtain a high-accuracy abundance estimation in this study. As a result, although the spectral fitting is not perfect, especially for endmember mixtures with biotite and natural granite, the Hapke model calibrated in this study is still suited for determining the modal mineralogy of synthetic granite samples and unsorted powder samples of natural granite. Interestingly, although the Hapke model is optimized for particulate media, our testing results involving bulk slab granite samples were also promising, except for the Qtz and Kfs endmembers with errors in abundance estimation greater than 10%, clearly demonstrating that the Hapke model can also be effectively applied to estimate the mineral abundance of terrestrial granite. The decreased accuracy determined in the case of natural granite is due to the change in the optical properties of the bulk slab and unsorted powder samples compared to that of the synthetic (endmember minerals) samples. For the typical nonlinear mixture model designed to deal with intimate mixtures, e.g., the synthetic (endmember minerals) samples in this study, particles are assumed to be fundamentally mono-minerally, with void spaces that affect the material's scattering properties present between grains (Hapke, 1993), while the bulk unsorted powder samples are multimineral particles, representing a more complex system to model accurately. For the bulk slab sample, the constituents also interact in a complex manner such that the coherent interactions between particles are no longer nonnegligible (Hapke, 2008), and the effects of the close packing of the bulk slab samples remain to be explored.

Spectral unmixing models based on the radiative transfer model rely on accurate knowledge of the endmember spectra used (Isaacson et al., 2011). In our study, the endmember minerals used in the abundance estimation were extracted from the exact bulk sample being analyzed, which is critical for building endmember spectral libraries. Thus, the high-quality endmember spectra can exactly match the minerals found in the measured sample under study and thus improve the accuracy of estimation. Furthermore, the endmember spectra studied in this paper can likely be extended to the existing VNIR-SWIR spectrum library. However, we realize

that in natural granite, the presence of a range of minor constituent minerals besides the selected three endmembers could also lead to inaccuracies in the abundance estimation.

The ratios of Pl to Kfs in the synthetic mixtures are based on the QAPF diagram, which is expected to be compositionally similar to natural granite. The Hapke model accurately estimated the endmember mineral abundance of synthetic mixtures and natural granite with different feldspar ratios. At seven mixing ratios, the endmember abundances were predicted with similar accuracies. These results suggest that our current implementation of the Hapke model may be favored for the detailed mapping of terrestrial granite using VNIR-SWIR data.

4.4. Potential of the proposed approach for remote sensing applications of natural granite

Feldspar (plagioclases and K-feldspar) and quartz are typically difficult to detect only using spectral absorption features in the VNIR-SWIR ranges or when they are embedded in a matrix with more spectroscopically active minerals. However, the new method based on the photometric parameters (ω, b, and c) of the Hapke model retrieved from multiangle reflectance measurements, as performed in this study, can effectively estimate the abundance and particle size of the main rock-forming minerals (Qtz, Pl, and Kfs), even when only VNIR-SWIR wavelengths are used. Compared with previous studies using optical constants to estimate mineral abundance (Lucy, 1998; Li et al., 2015; Robertson et al., 2016; Warell & Davidsson, 2010), the proposed method in this paper is more suitable for natural granite and can reduce the uncertainty of estimated results. Since the optical constant is a feature of a monomineral, which is a mineral at the end of a solid solution from a geological perspective (Nickle, 1992), it is certainly inappropriate to directly use the optical constant derived from the pure monomineral to estimate the mineral composition in terrestrial rocks that are complex associations of endmember minerals. In particular, pure K-, Na-, and Ca- feldspar endmembers are difficult to find in nature (Matteson & Herron, 1993). In this study, we directly separated minerals from slab granite, which is the true endmember of the measured samples instead of considering monominerals as endmembers, allowing for accurate estimates of abundance. The reflectance spectra of minerals separated within different grain sizes, synthetic and natural granite should hence provide invaluable data sets for current and future terrestrial/extraterrestrial remote sensing exploration targeting granite.

5 Conclusions

We conducted a spectroscopy analysis of a suite of terrestrial granite with a variety of particle sizes. The measured spectra of four different kinds of samples provide incompatible controlled ground truths to conduct terrestrial granite mapping from reflected information. The proposed approach of spectral unmixing based on the Hapke model provides a good method to estimate the abundance and grain size of endmember minerals for both natural and synthetic granite samples. Photometric parameters retrieved from multiangle measurements are more suitable for unmixing complex mixtures with different minerals. The results suggest that our method will provide a feasible way to quantitatively estimate of the composition of terrestrial granite.

Acknowledgments

- The authors declare no conflict of interest.

- The authors would like to thank Zhongqiu Sun for providing the Northeast Normal University Laboratory Goniospectrometer System to measure the bidirectional reflectance of samples. The authors would also like to thank the Professional Laboratory for Geochemical Analysis and Testing, Xinjiang Institute of Ecology and Geography, CAS for providing the microscope to carry out the identification of thin sections.
- This work was supported in part by the Key Area Deployment Project of the Chinese Academy of Sciences, grant number ZDRW-ZS-2020-4-3 to Jinlin Wang, and by the National Natural Science Foundation of China, grant number U1803117 to Jinlin Wang.
- The bidirectional reflectrance spectral data have been included in supporting information.

References

Adams, J. B. (1974), Visible and near-infrared diffuse reflectance spectra of pyroxenes as applied to remote sensing of solid objects in the solar system. *Journal of Geophysical Research*, 79, 4829–4836. doi:10.1029/JB079i032p04829

Adams, J. B., & Filice, A. L. (1967), Spectral reflectance 0.4 to 2.0μm of silicate rock powders. *Journal of Geophysical Research*, 72, 5705–5715. doi.10.1029/JZ072i022p05705

Adams, J. B., & Goullaud, L. (1978), Plagioclase feldspars - Visible and near infrared diffuse reflectance spectra as applied to remote sensing. Proceedings of the Lunar and Planetary Science Conference 9th. doi. 10.1029/91GL01008

Bonin, B., Bébien, J., & Masson, P. (2002), Granite: A planetary point of view. *Gondwana Research*, 5, 261–273. doi.org/10.1016/S1342-937X(05)70722-X

Britt, D. T. (1991), The meteorite record as clues to asteroidal regolith processes. PhD. Dissertation, Brown University.

Britt, D. T., & Pieters, C. M. (1989), The physical, chemical, and spectral properties of opaque phases in optically altered ordinary chondrites. *Bulletin of the American Astronomical Society*, 21(3), 967.

Chandrasekhar, S. (1960), Radiative Transfer. Dover, New York.

Chen, S. Constrained Particle Swarm Optimization. MATLAB File Exchange, 2009-2018. https://www.mathworks.com/matlabcentral/fileexchange/25986

Clark, R. N. (1983), Spectral properties of mixtures of montmorillonite and dark grains - Implications for remote sensing minerals containing chemically and physically adsorbed water. *Journal of Geophysical Research*, 88, 10635–10644. doi.10.1029/JB088iB12p10635

Cloutis, E. A., Gaffey, M. J., Smith, D. G. W., & Lambert, R. S. J. (1990a), Metal silicate mixtures: Spectral properties and applications to asteroid taxonomy. *Journal of Geophysical Research*, 95(B6), 8323–8338. doi. 10.1029/JB095iB06p08323

Cloutis, E. A., Gaffey, M. J., Smith, D. G. W., & Lambert, R. S. J. (1990b), Reflectance spectra of glass-bearing mafic silicate mixtures and spectral deconvolution procedures. *Icarus*, 86, 383–401. doi.10.1016/0019-1035(90)90226-Y

De Angelis, S., Manzari, P., De Sanctis, M. C., Altieri, F., Carli, C., & Agrosì, G. (2017), Application of spectral linear mixing to rock slabs analyses at various scales using Ma_Miss

BreadBoard instrument. *Planetary and Space Science*, 144, 1–15. doi.org/10.1016/j.pss.2017.06.005

Freek, V. D. M. (2018), Near-infrared laboratory spectroscopy of mineral chemistry: A review. *International Journal of Applied Earth Observation and Geoinformation*, 65, 71–78. doi.org/10.1016/j.jag.2017.10.004

Gaffey, M. J. (1986), The spectral and physical properties of metal in meteorite assemblages: Implications for asteroid surface materials. *Icarus*, 66,468–486. doi. 10.1016/0019-1035(86)90086-2

Goudge, T. A., Mustard, J. F., Head, J. W., Salvatore, M. R., & Wiseman, S. M. (2015), Integrating CRISM and TES hyperspectral data to characterize a halloysite-bearing deposit in Kashira crater, Mars. *Icarus*, 250, 165–187. doi.10.1016/j.icarus.2014.11.034

Hapke, B. (1993), Theory of Reflectance and Emittance Spectroscopy. Cambridge University Press, Cambridge. doi.10.1017/CBO9780511524998

Hapke, B. (2008), Bidirectional reflectance spectroscopy: 6. Effects of porosity. *Icarus*, 195, 918–926. doi.10.1016/j.icarus.2008.01.003

Hunt, G. R. (1977), Spectral signatures of particulate minerals, in the visible and near-infrared. *Geophysics*, 42, 501–513. doi.10.1190/1.1440721

Isaacson, P. J., Sarbadhikari, A. B., Carlé, M. P., Rachel, L. K., Hiroi, T., Liu, Y., & Taylor, L.,A. (2011), The lunar rock and mineral characterization consortium: Deconstruction and integrated mineralogical, petrologic, and spectroscopic analyses of mare basalts. *Meteoritics & Planetary Science*, 46(2), 228–251. doi. 10.1111/j.1945-5100.2010.01148.x

Jacquemoud, S., Baret, F., & Hanocp, J. F. Modeling spectral and bidirectional soil reflectance. *Remote Senseing of Environment*, 41, 123–132. doi.10.1016/0034-4257(92)90072-R

Keshava, N., & Mustard, J. F. (2002), Spectral unmixing. *IEEE Signal Processing Magazine*, 19(1), 44–57. doi.10.1109/79.974727

Lapotre, M. G. A., Ehlmann, B. L., & Minson, S. E. (2017), A probabilistic approach to remote compositional analysis of planetary surfaces. *Journal of Geophysical Research Planets*, 122, 983–1009. doi. 10.1002/2016JE005248

Le Maitre, R. W. (1989), A classification of igneous rocks and glossary of terms. In Recommendations of the IUGS Subcommission on the Systematics of Igneous Rocks. Blackwell Scientific Publications, Oxford, 193. doi:10.1017/CBO9780511535581.005

Li, S., & Milliken, R. E. (2015), Estimating the modal mineralogy of eucrite and diogenite meteorites using visible-near infrared reflectance spectroscopy. *Meteoritics & Planetary Science*, 50, 1821–1850. doi. 10.1111/maps.12513

Liu, D., Li, L., & Sun, Y. (2015), An improved radiative transfer model for estimating mineral abundance of immature and mature lunar soils. *Icarus*, 253, 40–50. doi.org/10.1016/j.icarus.2015.02.013

Lucey, P. G. (1998), Model near-infrared optical constants of olivine and pyroxene as a function of iron content. *Journal of Geophysical Research Planets*, 103, 1703–1713. doi.org/10.1029/97JE03145

Matteson, A., & Herron, M. M. (1993), End-member feldspar concentrations determined by FTIR spectral analysis. *Journal of Sedimentary Petrology*, 63(6), 1144–1148. doi.10.1306/D4267CC6-2B26-11D7-8648000102C1865D

Mustard, J. F., & Hays, J. E. (1997), Effects of hyperfine particles on reflectance spectra from 0.3 to 25 μm. *Icarus*, 125(1), 145–163. doi.10.1006/icar.1996.5583

Mustard, J. F., & Pieters, C. M. (1978a), Quantitative abundance estimates from bidirectional reflectance measurements. *Journal of Geophysical Research*, 92(B4), E617–E626. doi.org/10.1029/JB092iB04p0E617

Mustard, J. F., & Pieters, C. M. (1987b), Abundance and distribution of ultramafic microbreccia in Moses Rock dike: Quantitative application of mapping spectroscopy. *Journal of Geophysical Research Planets*, 92(10), 376–390. doi. 10.1029/JB092iB10p10376

Mustard, J. F., & Pieters, C. M. (1989), Photometric phase functions of common geologic minerals and applications to quantitative analysis of mineral mixture reflectance spectra. *Journal of Geophysical Research*, 94(13), 619–634. doi.org/10.1016/0148-9062(90)94425-S

Nickel, E. H. (1992), Solid solutions in mineral nomenclature. *Mineralogy and Petrology*, 46, 49–53. doi.10.1007/BF01160701

Pilorget, C., Fernando, J., Ehlmann, B. L., & Douté, S. (2015), Photometry of particulate mixtures: What controls the phase curve? *Icarus*, 250, 188–203. doi.org/10.1016/j.icarus.2014.11.036

Poulet, F., Cuzzi, J. N., Cruikshank, D. P., Roush, T. L., & Dalle Ore, C. M. (2002), Comparison between the Shkuratov and Hapke scattering theories for solid planetary surfaces: Application to the surface composition of two centaurs. *Icarus*, 160, 313–324. doi.10.1006/icar.2002.6970

Poulet, F., Ehlmann, B. L., Mustard, J. F., Vincendon, M., & Langevin, Y. (2010), Modal mineralogy of planetary surfaces from visible and near-infrared spectral data. In 2nd Workshop on hyperspectral image and signal processing: evolution in remote sensing. New York: IEEE., 1–4. doi:10.1109/WHISPERS.2010.5594898

Robertson, K. M., Milliken R. E., & Li, S. (2016), Estimating mineral abundances of clay and gypsum mixtures using radiative transfer models applied to visible-near infrared reflectance spectra. *Icarus*, 277, 171–186. doi:10.1016/j.icarus.2016.04.034

Serventi, G., Carli, C., Sgavetti, M., Ciarniello, M., Capaccioni, F., & Pedrazzi, G. (2013), Spectral variability of plagioclase–mafic mixtures (1): Effects of chemistry and modal abundance in reflectance spectra of rocks and mineral mixtures. *Icarus*, 226(1), 282–298. doi. 10.1016/j.icarus.2013.05.041

Shkuratov, Y. G., Kreslavsky, M. A., Ovcharenko, A. A., Stankevich, D. G., Zubko, E. S., Pieters, C., & Arnold, G. (1999), Opposition effect from clementine data and mechanisms of backscatter. *Icarus*, 141, 132–155. doi.10.1006/icar.1999.6154

Sklute, E. C., Glotch, T. D., Piatek, J. L., Woerner, W. R., Martone, A. A., & Kraner, M. L. (2015), Optical constants of synthetic potassium, sodium, and hydronium jarosite. *American Mineralogist*, 100, 1110–1122. doi.10.2138/am-2015-4824

Streckeisen, A. (1968), Account of classification and nomenclature of igneous rocks. Reprent of 23rd International Geological Congress Prague.

Sun, Z., Wu, Z., & Zhao, Y. (2014), Semi-automatic laboratory goniospectrometer system for performing multi-angular reflectance and polarization measurements for natural surfaces. *Review of Science Instruments*, 85, 014503. doi.10.1063/1.4862814

Wang, H. (2015), Remote sensing methods research to identify different granitoids. Ph.D. dissertation, China University of Geosciences (Beijing).

Warell, J., & Davidsson, B. J. R. (2010), A Hapke's model implementation for compositional analysis of VNIR spectra of Mercury. *Icarus*, 209, 164–178. doi.10.1016/j.icarus.2009.11.037

Wu, M., Wang, J., Wang, Q., Zhou, K., Zhang, Z., Ma, X., & Chen, W. (2020), Retrieval of particle size of natural granite from multiangular bidirectional reflectance spectra using the Hapke model. *IEEE Transactions on Geoscience and Remote Sensing*, in press. doi.10.1109/TGRS.2020.3030101

Yang, Y., Li, S., Milliken, R. E., Zhang, H., Robertson, K., & Hiroi, T. (2019), Phase functions of typical lunar surface minerals derived for the Hapke model and implications for visible to near-infrared spectral unmixing. *Journal of Geophysical Research Planets*, 124, 31–60. doi.10.1029/2018JE005713